

Symmetry-based perturbation theory for electronic structure calculations

Hironichi Nishimura^{*1}, Nam Nguyen¹, Tanvi Gujarati², and Mario Motta³

¹Applied Mathematics, Boeing Technology Innovation, Huntington Beach, CA 92647, USA

²IBM Quantum, IBM Almaden Research Center, San Jose, CA 95120, USA

³IBM Quantum, IBM T. J. Watson Research Center, Yorktown Heights, NY 10598, USA

March 10, 2026

Abstract

We develop a multi-reference perturbation theory for electronic structure calculations based on symmetries of the Hamiltonian. The reference Hamiltonian in the symmetry-based perturbation theory (SBPT) is chosen such that it possesses more symmetries than the original Hamiltonian, leading to a larger reduction of computational resources in terms of both the number of configurations in the configuration interaction expansion and the number of required qubits in quantum computing applications. We provide approximate, scalable solutions for the second-order correction, as well as an application to selected configuration interaction. We show that SBPT is an extension of other existing multi-reference perturbation theories and that it can give better results for some molecular systems in a robust way.

1 Introduction

Computing the electronic structure of molecular systems is of great importance in both fundamental science and industry. It can explain the behavior and properties of molecules and can guide the search for new materials. Designs for corrosion-resistant materials, drugs, and batteries, for example, can be aided by computational chemistry to accelerate the search for better products through experiments [1, 2, 3, 4, 5, 6].

Ab initio calculations to solve the electronic structure problem use the Schrödinger equation for N -electron systems with fixed nuclei. Exact solutions for molecular systems do not exist, except in special circumstances like non-interacting systems and the Bethe ansatz for one-dimensional systems [7]. Even exact numerical solutions by the full configuration interaction (FCI) method are approximated, as they are only exact within a finite basis set. The exact solution is, however, not necessary or even relevant in many cases; achieving sufficient accuracy for the properties of interest is what matters. One of the goals of quantum chemistry is to model or approximate a molecular system such that we can capture the correct physics and obtain a result with desired accuracy.

Perturbation theory (PT) is one of many approximation methods with substantially low computational cost. It first solves a reference Hamiltonian by ignoring part of the Hamiltonian, and then it incorporates perturbative corrections using expansions such as asymptotic series. There are now many perturbation methods that differ by the reference Hamiltonian, but they can be categorized as either single-reference PT (SRPT) or multi-reference PT (MRPT). In a SRPT, such as Moller-Plesset PT [8] and Epstein-Nesbet PT [9, 10], a solution to the reference Hamiltonian is a single electron configuration. A single mean-field wave function such as the Hartree-Fock (HF) state is a good approximation to a solution for single-reference systems, and a SRPT typically gives accurate results with very low cost.

Many interesting problems, however, require a multi-reference description and thus invalidate single-reference approaches. They include bond breaking, transition metal complexes, magnetic systems, and

^{*}hironichi.nishimura@boeing.com

excited states [11, 12, 13, 14, 15, 16, 17]. MRPTs aim to overcome the issue by increasing the size of the reference Hamiltonian. Solutions to the reference Hamiltonian in standard MRPTs are typically full solutions in a smaller orbital basis called complete active space (CAS). A standard MRPT theory based on CAS, such as CAS perturbation theory (CASPT) [18] and *n*-electron valence state perturbation theory (NEVPT) [19, 20, 21], is designed such that the reference Hamiltonians can capture strong (static) correlations, while perturbative corrections incorporate weak (dynamical) correlations. The partition of the Hamiltonian aims to encapsulate correct physics in the reference Hamiltonian while obtaining accurate results through a perturbative expansion. The method can be systematically improved as we increase the size of the CAS in exchange for a larger computational cost, and it becomes exact as CAS approaches FCI.

Quantum computing is yet another approach that could obtain high-fidelity results with low computational cost. For example, quantum phase estimation (QPE) [22] could provide a result comparable to FCI with only polynomial time complexity on a noiseless quantum computer, thus possibly achieving a computational speedup [23]. Fault-tolerant implementation to achieve optimal complexity in the presence of errors relies heavily on efficient algorithms for quantum time evolution and state preparation, and it is an active research area. As a heuristic method, the quantum computing application to the electronic structure problems is possible without error correction for noisy intermediate-scale quantum (NISQ) devices. The NISQ algorithms aim to prepare states of interest with a quantum circuit depth that is orders of magnitude shallower than QPE by introducing variational parameters in the variational quantum eigensolver (VQE) [24] or by employing approximate circuits such as the LUCJ ansatz [25]. There are now many NISQ algorithms for electronic structure problems, and some well-studied ones include the Krylov method [26, 27], quantum selected configuration interaction (QSCI) [28, 29, 30, 31, 32], and sample-based quantum diagonalization (SQD) [33, 34, 35, 36, 37, 38, 39]. As another heuristic method, the implementation of NEVPT in quantum computing applications has been studied in [40, 41].

This paper can be seen as another quantum computing application of perturbation theory in quantum chemistry. But there is more. We introduce a new MRPT by extending the existing MRPT framework. Our proposed reference Hamiltonian is constructed from symmetry considerations, and we call this symmetry-based perturbation theory (SBPT). We review the symmetry of the electronic Hamiltonian in Sec. 2 and show how we can exploit the symmetry to construct the reference Hamiltonian in Sec. 3. Our approach can be used as a classical or quantum computational method.

\mathbb{Z}_2 symmetry is particularly important because of the adaptation of qubit tapering, as discussed in 4.2. We also discuss the implementation of selected configuration interaction (SCI) to circumvent the shortcomings of perturbation theory in Sec. 4.1. We demonstrate our methods on some small molecular systems in Sec. 5. These results can be obtained exactly through quantum computations in a noiseless simulation with significant resource reductions. Our initial study focuses on simple molecules to demonstrate the outperformance of SBPT over other MRPT methods in a concrete way. We then conclude in Sec. 6.

2 Symmetries of the electronic Hamiltonian

In this section, we establish our notations and review the aspects of symmetry in quantum chemistry needed for this paper. For more details, readers can refer to [42, 43] for molecular orbital theory and [44, 45] for point group symmetries.

We consider the electronic structure of a molecule, where the nuclei are treated as stationary using the Born-Oppenheimer approximation. The Hamiltonian, called the electronic Hamiltonian, in atomic units is then given by

$$H = -\sum_i \frac{1}{2} \nabla_i^2 - \sum_{i,l} \frac{Z_l}{|\mathbf{r}_i - \mathbf{R}_l|} + \sum_{i>j} \frac{1}{|\mathbf{r}_i - \mathbf{r}_j|} \quad (1)$$

where \mathbf{R}_l and Z_l are the position and the atomic number of *l*-th nucleus, and \mathbf{r}_i is the position of the *i*-th electron. One of the goals in quantum chemistry is to solve the eigensystem, namely for the *n*-th eigenvalue of the Hamiltonian:

$$H |\Psi_n\rangle = E_n |\Psi_n\rangle \quad (2)$$

where the eigenstate $|\Psi_n\rangle$ is an *N*-electron wavefunction, which is a function of the spatial and spin degrees of freedoms for *N* electrons.

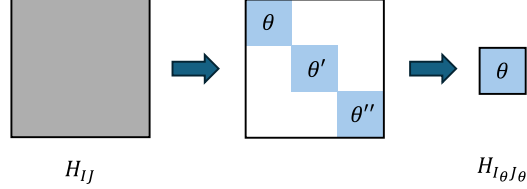


Figure 1: The matrix on the left is a $D \times D$ Hamiltonian matrix, $H_{IJ} = \langle \Phi_I | H | \Phi_J \rangle$. The Hamiltonian can be reduced to a block diagonal form using the symmetries of H , where unshaded elements are all zero. Each block matrix is labeled by its irreducible representation θ and given by a $D_\theta \times D_\theta$ matrix, $H_{I_\theta J_\theta} = \langle \Phi_{I_\theta} | H | \Phi_{J_\theta} \rangle$.

Symmetries – The eigenstate exhibits two different kinds of symmetries. First it is antisymmetric with respect of the exchange of two electrons due to the spin-statistics theorem for fermions. This property makes the eigenvalue problem notoriously difficult: for example, it gives rise to the sign problem in quantum Monte Carlo simulations. Second it respects the symmetries of the electronic Hamiltonian. We consider three symmetries in the electronic Hamiltonian: $U(1)$ charge symmetry, $SU(2)$ spin symmetry, and a point group symmetry. We will discuss each symmetry in a little more detail below. The unitary operator U_a , labeled by a and belonging to the symmetry group, commutes with the Hamiltonian, $[H, U_a] = 0$. Therefore the eigenstate is an irreducible representation θ of the symmetry group, and we now denote the n -th eigenstate in the irrep θ as $|\Psi_{n_\theta}\rangle$. We use the terms irreducible representation and irrep interchangeably. This reducibility can restrict the form of the N -electron wavefunction and simplify the problem.

To illustrate how we typically take advantage of the symmetry, we consider a set of N -electron wavefunctions $|\Phi_I\rangle$ with $I = 1, 2, \dots, D$ as basis functions. The finite basis approximation is necessary except in special exactly-solvable cases, such as the hydrogen atom. To obtain the eigenvalues, we simply diagonalize the $D \times D$ Hamiltonian matrix, $H_{IJ} = \langle \Phi_I | H | \Phi_J \rangle$. On the other hand, if we can choose a finite set of basis functions that capture the symmetry of the Hamiltonian, then we can completely reduce it to a block diagonal form, where the basis functions are now in an irreducible representation, $|\Phi_{I_\theta}\rangle$ with $I_\theta = 1, 2, \dots, D_\theta$. We use the same notation Φ for brevity, but the new basis $|\Phi_{I_\theta}\rangle$ can be a linear combination of the original basis $|\Phi_I\rangle$: one such example is the configuration state function basis mentioned below. In this new basis, we only need to diagonalize the subspace $H_{I_\theta J_\theta} = \langle \Phi_{I_\theta} | H | \Phi_{J_\theta} \rangle$ to obtain the n_θ -th eigenstate $|\Psi_{n_\theta}\rangle$:

$$|\Psi_{n_\theta}\rangle = \sum_{I_\theta} c_{I_\theta} |\Phi_{I_\theta}\rangle. \quad (3)$$

This reduction process is illustrated in Fig. 1. The symmetry of the electronic Hamiltonian can therefore reduce the computational cost of solving the eigensystems, if we can construct the basis functions in the irreducible representations $|\Phi_{I_\theta}\rangle$. Next, we discuss how to construct such bases.

Basis states – One way to construct a basis set of N -electron wavefunctions in general is to start from a set of one-electron wavefunctions. A one-electron wavefunction is a product of a spatial orbital function ϕ_p and a spin function: together it is called a spin orbital. We denote the spin orbital as ψ_p . An N -electron wavefunction can be then constructed by the antisymmetrization of a tensor product of N spin orbitals, called a Slater determinant or a configuration.

In this paper, we only consider an abelian subgroup S of the symmetry in the electronic Hamiltonian. The reason is that we can then construct every Slater determinant in an irreducible representation of the abelian subgroup. The $SU(2)$ spin symmetry, for example, is non-abelian. For the restricted determinant where the spatial orbitals are the same for spin up and down, one can construct a spin eigenstate using a symmetry-adapted linear combination (SALC) of Slater determinants. This SALC is called a spin-adapted configuration or a configuration state function (CSF). In general, irreducible representations of a non-abelian group cannot be written as a single Slater determinant and require a SALC of multiple Slater determinants. While the use of SALC reduces the dimension of the Hamiltonian matrix, it may not be easy or computationally efficient to construct such a basis. There is, however, a recent development in quantum computing application to prepare ground states efficiently using CSFs in the quantum subspace expansion [46].

The $U(1)$ charge symmetry, which is abelian, gives rise to the conservation of the total number N of electrons. It is clear that the Slater determinant is already an eigenstate of the number operator \hat{N} . In

general, when the number of electrons N_a in a set L_a of spin orbitals is conserved, such as spin up (\uparrow) or spin down (\downarrow) due to the $U(1)$ subgroup of $SU(2)$ spin symmetry, the corresponding unitary symmetry operation is a $U(1)$ rotation. To compute a spin singlet eigenstate, for example, we only need to consider the Slater determinants $|\Phi_{I_\theta}\rangle$ with the eigenvalues $N_\uparrow = N_\downarrow = N/2$. The number of relevant configurations grows factorially rather than exponentially due to the $U(1)$ symmetries.

The other symmetry, point group symmetry, is present when a molecule has a symmetric spatial structure, which is invariant under coordinate transformations such as rotations or inversions. To construct spatial orbitals, we typically employ a set of atomic orbitals and use a linear combination of them. We then minimize the energy of a Slater determinant as a function of its occupied orbitals self-consistently using the Hartree-Fock (HF) equation. Since the HF equation respects the point-group symmetry of the full Hamiltonian, the converged solutions should be in the irreducible representation of the point group. We can enforce this condition by using the projection operator to construct SALCs of atomic orbitals. Again we only consider the unitary representation of the abelian subgroup of the point group symmetry.

An irreducible representation is defined by its characters on the conjugacy classes of the group, i.e. corresponding to a row in the character table for the point group symmetry. For abelian groups, every irrep is one dimensional and is uniquely determined by its characters, or equivalently eigenvalues, of the group generators. Acting a unitary operator U_a in the abelian group S on a spin orbital ψ_p , we have $U_a |\psi_p\rangle = e^{i\theta_p(a)} |\psi_p\rangle$, where $e^{i\theta_p}$ is the character. Acting the operator on the N -electron Slater determinant, we obtain

$$U_a |\Phi_{I_\theta}\rangle = e^{i\theta(a)} |\Phi_{I_\theta}\rangle = \prod_{p \in L_a} e^{i\theta_p(a) \hat{N}_p} |\Phi_{I_\theta}\rangle \quad (4)$$

where \hat{N}_p is the number operator for the spin orbital ψ_p , and L_a is a set of orbitals that have a non-trivial character, i.e., $\theta_p(a) \neq 0$ for $p \in L_a$. For the Slater determinant $|\Phi_{I_\theta}\rangle$ in an irrep θ , the number of electrons occupying in the set L_a is constrained by the equation,

$$\theta(a) = \sum_{p \in L_a} \theta_p(a) \langle \Phi_{I_\theta} | \hat{N}_p | \Phi_{I_\theta} \rangle \quad (5)$$

for each operator U_a . Again the equation is completely determined by the characters of the group generators. We can therefore construct Slater determinants as the N -electron basis functions $|\Phi_{I_\theta}\rangle$ in the 1D irrep of the abelian subgroup of the symmetries in the electronic Hamiltonian.

Second quantization – The matrix H_{IJ} is sparse because the electronic Hamiltonian Eq. (1) is a two-body Hamiltonian. For example, the coupling between two configurations with more than two different spin orbitals is zero by the Slater-Condon rules. For this reason, instead of explicitly constructing the full matrix H_{IJ} as in Fig. 1, we use the second-quantized Hamiltonian,

$$H = \sum_{pq} h_{pq} a_p^\dagger a_q + \frac{1}{2} \sum_{pqrs} h_{pqrs} a_p^\dagger a_q^\dagger a_r a_s. \quad (6)$$

This is an efficient way to store the same information without computing all nonzero elements of the Hamiltonian matrix. The coefficients h_{pq} and h_{pqrs} are the one-body and two-body integrals:

$$h_{pq} = \langle \psi_p | \left(-\frac{\nabla^2}{2} - \sum_l \frac{Z_l}{|\mathbf{r} - \mathbf{R}_l|} \right) | \psi_q \rangle \quad (7)$$

$$h_{pqrs} = \langle \psi_p \psi_q | \frac{1}{|\mathbf{r} - \mathbf{r}'|} | \psi_r \psi_s \rangle$$

where $|\mathbf{r} - \mathbf{r}'|$ is the distance between the two electrons and the operator a_p^\dagger/a_q creates/destroys an electron in the spin-orbital p/q .

The unitary operator U_a commutes not only with the Hamiltonian, $[H, U_a] = 0$, but also with each fermionic operator, $\mathcal{O} = a_p^\dagger a_q$ or $a_p^\dagger a_q^\dagger a_r a_s$, in the second-quantized Hamiltonian,

$$[\mathcal{O}, U_a] = 0. \quad (8)$$

The reason is the following. For any basis function $|\Phi_{I\theta}\rangle$ in the irrep θ , the operation of $a_p^\dagger a_q$ or $a_p^\dagger a_q^\dagger a_r a_s$ transforms it to another basis function in the same irrep θ , because $\theta_p = \theta_q$ or $\theta_p + \theta_q = \theta_r + \theta_s$, respectively, from the definition of one-body and two-body integrals above. Any algorithm that uses fermionic operators in the Hamiltonian, such as the FCI calculation of the ground state energy with Davidson’s method or what we discuss in this paper, ensures computation in the subspace of the irreducible representation, and this is again the consequence of symmetry reduction.

3 Symmetry-based perturbation theory

As we have discussed in the previous section, the symmetries of the electronic Hamiltonian can be used to reduce computational cost. We now propose a new perturbative method, where the choice of the reference Hamiltonian is guided by the symmetry. The idea of symmetry-based perturbation theory (SBPT) is simple: we split the second quantized Hamiltonian in Eq. (6) into two parts,

$$H = H_{\text{ref}} + H_{\text{pert}} \quad (9)$$

such that the reference Hamiltonian H_{ref} has a larger abelian group S_{ref} than the original abelian group S .

In this section, we develop this idea. We first consider the types of approximate symmetries relevant for SBPT in Sec. 3.1. We then show how we split the Hamiltonian based on the approximate symmetry in Sec. 3.2 and compute the second-order correction in Sec. 3.3. Lastly we discuss the relation to other multi-reference perturbation theories in Sec. 3.4 and possible issues in Sec. 3.5.

3.1 Approximate symmetries

We consider an orbital energy diagram shown in Fig. 2, where the horizontal black line indicates a spin orbital ψ_p . The solid box indicates a set L_a of spin orbitals, where the number of electrons N_a occupying the spin orbitals in the full configuration interaction (FCI) is constrained due to the exact abelian symmetry S , reducing the number of possible Slater determinants as discussed in the previous section.

Suppose that there is another set L_b of orbitals that are nontrivially coupled, as indicated by a dashed box. A nontrivial coupling means that the number of electrons N_b occupying the set L_b is approximately constrained in the FCI. There are at least two cases in which the orbitals are nontrivially coupled: (I) The orbitals transform nontrivially under an approximate point-group symmetry. (II) The orbitals couple weakly with the rest of the orbitals.

The first case (I) may occur when the geometry is slightly deviated from the symmetric structure. We study such a case in Sec. 5.1. It is then natural to construct a reference Hamiltonian that makes the approximate symmetry exact. For the second case (II), we point out that the total number of electrons N_b is conserved if the spin orbitals ψ_p with $p \in L_b$ do not couple at all with the rest of the orbitals, ψ_q with $q \notin L_b$. By treating a small interaction between the ψ_p and the rest of the orbitals as a perturbation, the total number of electrons in L_b is conserved in the reference Hamiltonian, which then possesses a new symmetry for the particle number.

In this regard the two cases are the same from the symmetry perspective. The first case (I) promotes the approximate point-group symmetry to the exact one, while the second case (II) creates a new particle number symmetry in the reference Hamiltonian. In either case, we make the approximate symmetry as an exact symmetry and construct the reference Hamiltonian that respects the new augmented symmetry S_{ref} , as illustrated in the orbital energy diagram with a new solid box on the right in Fig. 2.

3.2 Optimal partitioning

Given a new augmented symmetry S_{ref} , the idea of SBPT is to split the Hamiltonian as in Eq. (9), where every fermionic operator \mathcal{O}_{ref} in H_{ref} has the commutation relationship $[\mathcal{O}_{\text{ref}}, U_a] = 0$ for any symmetry operator U_a in S_{ref} . It is easy to see that the reference Hamiltonian in this construction is not unique.

We can further require that each fermionic operator $\mathcal{O}_{\text{pert}}$ in H_{pert} does not commute with at least one of the new symmetry operators. That is, we require that each fermionic operator in H_{pert} satisfies

$$[\mathcal{O}_{\text{pert}}, U_a] \neq 0 \quad (10)$$

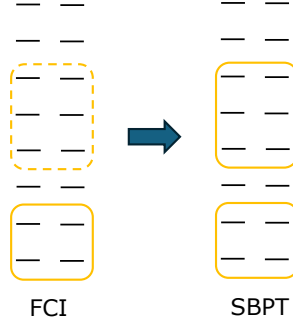


Figure 2: A schematic orbital energy diagram, with each horizontal black line representing a spin orbital ψ_p . The orbitals in the solid box transform nontrivially under a symmetry operation in the abelian group. The number of such operations and the number of solid boxes in SBPT are greater than in FCI - the more the number of boxes, the smaller the computational cost to solve for the reference Hamiltonian.

for some U_a in S_{ref} . This additional requirement forbids adding a fermionic operator that respects S_{ref} into H_{pert} , or in other words, it ensures each operator in H_{pert} breaks S_{ref} . This means that each fermionic term in H_{pert} transforms a basis function $|\Phi_{I_\theta}\rangle$ in the irrep θ into another basis function $|\Phi_{I_{\theta'}}\rangle$ with a different irrep $\theta' \neq \theta$:

$$\mathcal{O}_{\text{pert}} |\Phi_{I_\theta}\rangle = \gamma |\Phi_{I_{\theta'}}\rangle \quad (11)$$

where $\theta' = \theta - \theta_q + \theta_p$ for $\mathcal{O}_{\text{pert}} = a_p^\dagger a_q$ and $\theta' = \theta - \theta_s - \theta_r + \theta_q + \theta_p$ for $\mathcal{O}_{\text{pert}} = a_p^\dagger a_q^\dagger a_r a_s$, and $\gamma = \pm 1$ or 0 .

The extra requirement in Eq. (10) is not necessary to perform the perturbative expansion, but it gives rise to a few desirable properties. First, for a given symmetry S_{ref} , it is clear that this is the optimal way to split the Hamiltonian, where the reference Hamiltonian uniquely gives the largest norm $\|H_{\text{ref}}\|$. We therefore call the way of splitting in Eq. (10) the optimal partitioning. Having a small norm for the perturbation is a necessary condition for a meaningful perturbative expansion at lower order. Other nice features include that the first-order correction is always zero, and we can make an efficient approximation for the second-order correction, as we show in the next subsection.

In order to compute the energy spectrum in an irreducible representation θ , it is convenient to write a Hamiltonian as $H = \sum_{\theta'} V_{\theta',\theta}$, where the fermionic operator in $V_{\theta',\theta}$ transforms a state of our interest in the representation θ into a state with θ' . In the optimal partitioning, we have $H_{\text{ref}} = V_{\theta,\theta}$, and

$$H_{\text{pert}} = \sum_{\theta' \neq \theta} V_{\theta',\theta} \quad (12)$$

where the summation is over θ' only and $\theta' = \theta$ is excluded. The number of fermionic operators in $V_{\theta',\theta}$ is at most the number of fermionic operators in H_{pert} , which grows only polynomially with the size of the problem. This fact is important for the higher-order corrections.

3.3 Perturbative expansion up to second order

The optimal partitioning in Eq. (10) defines a unique reference Hamiltonian for a given symmetry S_{ref} , and we can perform the standard time-independent Rayleigh-Schrödinger perturbation theory (PT). We consider an n -th state in an irreducible representation θ of the full Hamiltonian, denoted as $|\Psi_{n_\theta}\rangle$ with the energy E_{n_θ} , and perform the perturbative expansion up to the second-order correction using the optimal partitioning.

The leading order contribution of E_{n_θ} is an n -th eigenvalue of the reference Hamiltonian in the irreducible representation θ :

$$H_{\text{ref}} |\Psi_{n_\theta}^{(0)}\rangle = E_{n_\theta}^{(0)} |\Psi_{n_\theta}^{(0)}\rangle \quad (13)$$

where the superscript denotes the order of perturbative expansion. The augmented symmetry in H_{ref} can reduce the computational cost for this eigenvalue problem.

The first-order correction is given as the expectation value of H_{pert} with respect to the unperturbed state. Acting the V operator in Eq. (12) on the unperturbed state, we obtain an unnormalized state in an irreducible representation $\theta' \neq \theta$,

$$V_{\theta',\theta} \left| \Psi_{n_\theta}^{(0)} \right\rangle = \left| \Xi_{n_{\theta'}} \right\rangle. \quad (14)$$

Using this, we can show that (1) the leading-order contribution for the ground-state energy gives an upper bound, $E_0 \leq E_0^{(0)}$, due to the variational principle, $E_0 \leq \langle \Psi_0^{(0)} | H | \Psi_0^{(0)} \rangle = \langle \Psi_0^{(0)} | H_{\text{ref}} | \Psi_0^{(0)} \rangle = E_0^{(0)}$ and (2) the first-order correction is always zero,

$$E_{n_\theta}^{(1)} = \langle \Psi_{n_\theta}^{(0)} | H_{\text{pert}} | \Psi_{n_\theta}^{(0)} \rangle = \sum_{\theta' \neq \theta} \langle \Psi_{n_\theta}^{(0)} | \Xi_{n_{\theta'}} \rangle = 0, \quad (15)$$

because the states in different irreducible representations are orthogonal. The optimal partitioning is optimal not only because the norm of H_{pert} is the smallest for a given symmetry, but also because the first-order correction is already incorporated into the leading contribution, potentially reducing computation cost.

In the optimal partitioning, non-trivial contributions start from the second-order correction:

$$E_{n_\theta}^{(2)} = \sum_{\theta' \neq \theta} \sum_{m_{\theta'}} \frac{\left| \langle \Psi_{m_{\theta'}}^{(0)} | H_{\text{pert}} | \Psi_{n_\theta}^{(0)} \rangle \right|^2}{E_{n_\theta}^{(0)} - E_{m_{\theta'}}^{(0)}} = \sum_{\theta' \neq \theta} \sum_{m_{\theta'}} \frac{\left| \langle \Psi_{m_{\theta'}}^{(0)} | \Xi_{n_{\theta'}} \rangle \right|^2}{E_{n_\theta}^{(0)} - E_{m_{\theta'}}^{(0)}} \quad (16)$$

where we have used Eqs.(12), (14), and (15) in the second equality. This is a familiar expression for the second-order correction, only rewritten to show indices for irreducible representations.

The double summations indicate that we need all m -th excited states of H_{ref} in each irreducible representation $\theta' \neq \theta$. If the dimensions of irreducible representations are small, then it is possible to diagonalize each subspace to obtain the unperturbed excited states $|\Psi_{m_{\theta'}}^{(0)}\rangle$. Moller-Plesset PT is such an example, where the dimension is one, and the excited states are simply all possible Slater determinants. For multi-reference problems, the irreducible representation with a small dimension may fail to capture important configurations at the leading order, and the higher-order corrections may not be able to remedy this lack of multi-reference character. In these cases, it is crucial to contain many relevant configurations at leading order to capture the correct physics. Therefore the dimension of irreducible representations of H_{ref} needs to be sufficiently large, and as a result, obtaining all excited states becomes computationally demanding for multi-reference problems. Therefore we need to make an approximation for the second-order correction, just as in other multi-reference PTs.

There are several ways to approximate the second-order correction. All approaches use an approximation for the excited states to simplify the calculation. One approach is to use a mean-field approximation where we replace each excited state with a single Slater determinant,

$$E_{n_\theta}^{(2):\text{EN}} = \sum_{\theta' \neq \theta} \sum_{I_{\theta'}} \frac{\left| \langle \Phi_{I_{\theta'}} | H_{\text{pert}} | \Psi_{n_\theta}^{(0)} \rangle \right|^2}{E_{n_\theta}^{(0)} - E_{I_{\theta'}}} \quad (17)$$

where $|\Phi_{I_{\theta'}}\rangle$ is the Slater determinant and $E_{I_{\theta'}} = \langle \Phi_{I_{\theta'}} | H | \Phi_{I_{\theta'}} \rangle$. This approximation is a generalization of the multi-reference Epstein-Nesbet PT as we discuss in Sec. 3.4, so we call this second-order correction the Epstein-Nesbet (EN) approximation. We could also improve this mean-field approximation by using excited states of another reference Hamiltonian with a small active space.

Another approach employs a contraction method, where we approximate the density matrix in Eq.(16) with a single state:

$$\sum_{m_{\theta'}} \left| \Psi_{m_{\theta'}}^{(0)} \right\rangle \left\langle \Psi_{m_{\theta'}}^{(0)} \right| \simeq \frac{\left| \Xi_{n_{\theta'}} \right\rangle \left\langle \Xi_{n_{\theta'}} \right|}{\left\langle \Xi_{n_{\theta'}} \right| \Xi_{n_{\theta'}} \right\rangle}. \quad (18)$$

This is analogous to the strongly contracted (SC) method in NEVPT. Using this contracted density matrix, the energy of the excited state in the θ' representation for H_{ref} is given as:

$$E_{n_{\theta'}}^{\text{SC}} = \frac{\left\langle \Xi_{n_{\theta'}} \right| H_{\text{ref}} \left| \Xi_{n_{\theta'}} \right\rangle}{\left\langle \Xi_{n_{\theta'}} \right| \Xi_{n_{\theta'}} \right\rangle} = E_{n_\theta}^{(0)} + \frac{\left\langle \Phi_{n_\theta}^{(0)} \right| V_{\theta',\theta}^\dagger [H_{\text{ref}}, V_{\theta',\theta}] \left| \Phi_{n_\theta}^{(0)} \right\rangle}{\left\langle \Xi_{n_{\theta'}} \right| \Xi_{n_{\theta'}} \right\rangle} \quad (19)$$

where we have used Eqs. (13) and (14) in the second equality, and the strongly contracted approximation for the correction, $E_{n_\theta}^{(2):\text{SC}} \simeq E_{n_\theta}^{(2)}$, becomes

$$E_{n_\theta}^{(2):\text{SC}} = \sum_{\theta' \neq \theta} \frac{\langle \Xi_{n_{\theta'}} | \Xi_{n_{\theta'}} \rangle}{E_{n_\theta}^{(0)} - E_{n_{\theta'}}^{\text{SC}}}. \quad (20)$$

This simplified approximation is possible because of Eq. (14), which is a direct consequence of the optimal partitioning. The computational cost for the strongly-contracted method is polynomial and it does not require any diagonalization – we discuss more about the scaling of the computational cost in Sec. 3.5.

3.4 \mathbb{Z}_2 symmetry-based PT and other multi-reference perturbation theories

In the previous subsection, we have seen some similarities between SBPT2 and NEVPT2. We denote a second-order perturbation theory as PT2. In this section, we show that SBPT is in fact an extension of other multi-reference perturbation theories (MRPTs) and argue why SBPT could perform better in certain situations.

In the rest of this paper, we restrict ourselves to \mathbb{Z}_2 symmetries. We consider a set L_a of spin orbitals where the number of electrons in L_a is either 0 or 1 modulo 2. The symmetry operator, whether it comes from the \mathbb{Z}_2 subgroup of point group symmetry or particle number symmetry, is then given by,

$$U_a = \prod_{p \in L_a} e^{i\pi \hat{N}_p} = \prod_{p \in L_a} (1 - 2a_p^\dagger a_p) \quad (21)$$

where $\hat{N}_p = a_p^\dagger a_p$ is the number operator for the spin orbital p . One could consider other abelian groups such as \mathbb{Z}_3 , but \mathbb{Z}_2 symmetry is the simplest and is also of great interest in the context of quantum computing applications as discussed in Sec. 4.2. For a given Slater determinant, its character $e^{i\theta(a)}$ is 1 if the number of electrons in L_a is even and -1 if it is odd. The irreducible representation is uniquely determined by a set of characters $\theta(a)$ on the generators U_a of the group. Moreover, the perturbation $V_{\theta', \theta}$ in Eq.(12) can be easily constructed for \mathbb{Z}_2 : the operator $\mathcal{O}_{\text{pert}}$ belongs to $V_{\theta', \theta}$ where $\theta'(a) = \theta(a)$ for $[\mathcal{O}_{\text{pert}}, U_a] = 0$ and $e^{i\theta'(a)} = -e^{i\theta(a)}$ for $[\mathcal{O}_{\text{pert}}, U_a] \neq 0$.

We now argue that some existing MRPTs are SBPT with \mathbb{Z}_2 symmetry. Let us assume that the four highest spin orbitals in a set L are weakly coupled, so that there is an approximate symmetry for the number of electrons in L . We again use a dashed box to indicate the approximate symmetry, as shown on the left in Fig. 3. Furthermore, we assume that each spin orbital in L does not couple much among themselves, and thus each has an approximate \mathbb{Z}_2 symmetry. This corresponds to four sets L_a with $a = 1, 2, 3, 4$ as illustrated by the four small boxes in the middle figure of Fig. 3. Performing SBPT for the four \mathbb{Z}_2 symmetries, we have the Slater determinants in the irreducible representation $\theta(a) = 0$ for all a as unperturbed wavefunctions, and the Slater determinants having a nonzero electron number $\theta'(a) \neq 0$ for some a are treated perturbatively. This is equivalent to standard MRPTs, where we compute complete active space (CAS) without the orbitals in L_a , i.e. the external orbitals, and treat the external orbitals as perturbation. If the Hartree-Fock state is the dominant contribution for the exact solution, then we can perform a SBPT where each spin orbital has \mathbb{Z}_2 symmetry, as illustrated on the right in Fig. 3. This corresponds to a standard single-reference perturbation theory (SRPT).

In fact, the SRPT based on the single Hartree-Fock (HF) state on the right figure of Fig. 3 with the optimal partitioning in Eq. (10) corresponds to the Epstein-Nesbet perturbation theory (ENPT). Since each spin orbital has \mathbb{Z}_2 symmetry, all the fermionic operators that destroy and create a same spin orbital belong to the reference Hamiltonian. On the other hand, the reference Hamiltonian of Moller-Plesset perturbation theory (MPPT) only contains one-electron operators, $H_{\text{ref}} = \sum_p \epsilon_p a_p^\dagger a_p$, which respect the same symmetry as ENPT, but this partitioning is not optimal due to the lack of two-electron operators.

The MRPT based on CAS in the middle figure of Fig. 3 with the optimal partitioning in Eq. (10) is a version of NEVPT discussed in [19]. Using their notation, the reference Hamiltonian is given as

$$H_{\text{ref}} = \mathcal{P}_{\text{CAS}} H \mathcal{P}_{\text{CAS}} + \sum_{l,k} \mathcal{P}_{S_l^k} H \mathcal{P}_{S_l^k} \quad (22)$$

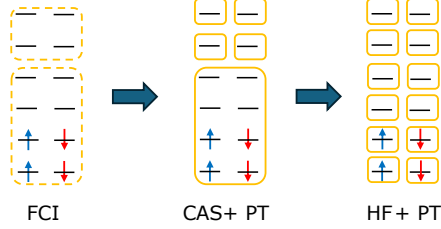


Figure 3: In this orbital energy diagram, the highest four spin orbitals couple weakly in FCI. In the middle figure, the standard MRPTs treat them as external orbitals and form a CAS with the rest of the orbitals. In other words H_{ref} has \mathbb{Z}_2 symmetries for each external spin orbital. The right figure corresponds to a situation where each spin orbital has \mathbb{Z}_2 symmetry, so that the HF state is the eigenstate of H_{ref} . The computational cost decreases as we make more approximations.

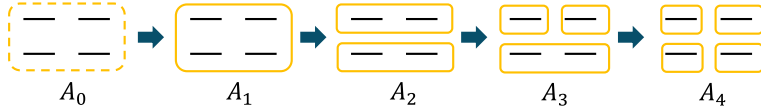


Figure 4: The four spin orbitals in A_0 couple nontrivially. Besides A_4 in standard MRPTs, SBPT can explore other groupings of \mathbb{Z}_2 symmetries, such as A_1 , A_2 , and A_3 shown here.

where \mathcal{P}_S is a projection operator onto the space S . The index k is the number of additional electrons in the active space, and l is the label for the electron configuration in the inactive orbitals, i.e. the orbitals that are not in the active space. Therefore their label (k, l) has a one-to-one correspondence with our label for the irrep θ' , both of which specify electron configurations in the inactive orbitals. If we employ the CAS and use the Epstein-Nesbet approximation in Eq. (17) for the second-order correction, the reference Hamiltonian becomes

$$H_{\text{ref}} = \mathcal{P}_{\text{CAS}} H \mathcal{P}_{\text{CAS}} + \sum_{\theta'} \sum_{I_{\theta'}} E_{I_{\theta'}} |\Phi_{I_{\theta'}}\rangle \langle \Phi_{I_{\theta'}}|. \quad (23)$$

This reference Hamiltonian was mentioned in the original NEVPT paper [19], and it is sometimes called the multi-reference Epstein-Nesbet perturbation theory in literature [47].

The standard NEVPT uses a model called the Dyll Hamiltonian for H_{ref} , but it employs the same symmetry and the optimal partitioning as the one in Eq. (22). On the other hand, CASPT uses the one-electron operator for H_{ref} similar to MPPT. In this case, there is a well-known issue called the intruder-state problem, where the energies of the perturber states are nearly degenerate with the energy of the unperturbed state. The perturbative term then becomes very large or singular, leading to divergent/oscillatory/unstable PT corrections [48, 49, 50, 51, 52, 53]. This is partly because the two-electron interaction is missing in the reference Hamiltonian. Our SBPT calculations are based on the optimal partitioning, and therefore they include all one and two-electron interactions that respect the symmetry. In the examples we studied, we did not encounter any intruder-state problems. In short, we find that all SRPTs and MRPTs discussed above can be seen as a version of \mathbb{Z}_2 SBPT with or without the optimal partitioning.

Framing MRPT in the language of SBPT, we find that the method to perform the standard MRPT may be restrictive, and there is a straightforward way to extend it. Suppose again that four spin orbitals are nontrivially coupled. We denote this grouping as A_0 as shown in Fig. 4. In this example, existing MRPT methods use the grouping A_4 , where each spin orbital has a \mathbb{Z}_2 symmetry as we discussed just above. On the other hand, there are many other ways to group the spin orbitals, depending on how they are coupled among themselves. We illustrate some examples of different grouping A_n for $n = 1, 2, 3$, where n is the number of \mathbb{Z}_2 symmetries. The larger the number n of grouping, the more symmetries we have to reduce the problem size. SBPT is therefore a generalization of MRPT, and it extends and opens up this new window of the grouping A_n of \mathbb{Z}_2 symmetries. Even when the standard MRPT using A_4 fails, the SBPT for different grouping A_n with $n = 1, 2, 3$ may give an accurate result. We demonstrate that this indeed happens in Sec. 5.

3.5 Possible issues in SBPT2

In this section, we discuss some of the possible issues we may face in SBPT2. First, as we increase the number of orbitals, there can be factorially many ways to form a grouping A_n for a given number of symmetries. Here we consider two methods to find a suitable grouping that may give a good result. First, the chemistry can guide us find nontrivially coupled orbitals by using the symmetries and the properties of orbitals. In general, finding a suitable grouping using chemistry knowledge may not be straightforward, and this is a similar situation as finding proper inactive orbitals in other standard MRPTs. Second, we can choose a grouping that gives a smaller norm of the perturbation Hamiltonian, $\|H_{\text{pert}}\|$. This will still give factorially many combinations, but it has an advantage of automating the search without the knowledge of the molecule. In practice, we use two approaches together. For example, if there are several suitable groupings from chemistry reasoning, we can choose the one that gives the smallest norm of H_{pert} . We will study this grouping for smaller molecular systems in Sec. 5 as an initial investigation.

Next, we provide a rough estimate of the computational cost for SBPT2. We first choose a complete active space $\text{CAS}(N, M)$, where N is the number of electrons and M is the number of orbitals. We then construct a reference Hamiltonian H_{ref} that possesses larger \mathbb{Z}_2 symmetries with K extra generators. The zeroth-order eigenvalue calculation requires the diagonalization of the D -dimensional H_{ref} matrix, where D is the number of determinants. Due to the augmented symmetry in H_{ref} , the number of determinants \tilde{N}_{det} in SBPT2 is smaller than the number N_{det} in $\text{CAS}(N, M)$. The actual number of determinants depends on the symmetry in H_{ref} , M , and N , but we have $\tilde{N}_{\text{det}}/N_{\text{det}} = 2^{-K}$ at best. The reason that it is typically less than 2^{-K} is because the number N_{det} of determinants is already reduced by the $U(1)$ symmetries mentioned in Sec. 2. Therefore the leading order calculation always favors SBPT2 over other MRPTs based on CAS. This advantage manifests as a reduction in qubit counts in the quantum computing application as explained in Sec. 4.2.

At second order, the majority of the computational cost in the strongly contracted method comes from the computation of Eq. (19). In NEVPT2, it requires the computational cost of the 4-RDM, which scales as $\mathcal{O}(M^8 N_{\text{det}})$, rather than the 6-RDM due to the commutation in Eq. (19) [20, 21, 53]. For the same fermionic operators in H_{pert} , we expect the same scaling but with a lower cost because the number of determinants is smaller, and the 8 indices in the 4-RDM are constrained by the symmetries.

There are, however, additional terms in H_{pert} due to the augmented symmetry. Consider a set L_a of spin orbitals that transform nontrivially under one extra generator. The number of extra terms in H_{pert} due to this extra generator scales as $M_a M^3$ where M_a is the number of orbitals in L_a . There are then $\sim M_a^2 M^8$ operators to compute in Eq. (19) after using the commutation. Again the number should be much smaller because the indices are constrained by the symmetries. For K extra generators, the total extra cost scales as $\mathcal{O}(\max(M_a)^2 K M^8 \tilde{N}_{\text{det}})$. This additional cost does not become a bottleneck as long as we have $\max(M_a)^2 K \tilde{N}_{\text{det}}/N_{\text{det}} \lesssim 1$. In general, we assume that $M_a \ll M$, or else the number K of extra symmetries becomes negligible compared to M . If $\max(M_a) \sim 1$, as we have in Sec. 5, then the condition $K \tilde{N}_{\text{det}}/N_{\text{det}} \lesssim 1$ should hold for any K .

Lastly we mention that the effectiveness of SBPT diminishes as the active space size M increases for a fixed number of symmetries. We will study this issue for the case of N_2 using two different basis set sizes in Sec. 5.2 and show that the number of symmetries can increase as we increase the basis size. We defer a more thorough investigation of all the issues above to future research.

4 Applications of SBPT

In this section, we consider two applications of SBPT. First we implement selected configuration interaction (SCI) in SBPT to overcome the shortcomings of perturbation theory. In the following section, we show that our method can be incorporated naturally into quantum computing applications to reduce the number of qubits using the so-called qubit tapering technique.

4.1 SCI-SBPT

The perturbative expansion for electronic structure calculations is an approximate method, which is typically neither convergent nor variational. A higher-order correction may result in a large error and/or a lower value

than the true ground-state energy. To circumvent these problems, we can employ selected configuration interaction (SCI) [54, 55, 56, 57] wherein the ground state is approximated by a sparse linear combination of electronic configurations [58, 59, 60, 61, 62, 63, 64, 65, 66, 67, 68].

The SCI selects important configurations and diagonalizes the matrix exactly within the selected subspace. A crucial aspect of SCI is to identify which configurations are most important. One of the common approaches is to use the second-order correction of Moller-Plesset perturbation theory as a selection criterion. This method can be naturally extended to SBPT.

We consider the strongly-contracted approximation of the second-order correction given in Eq. (20),

$$E_{n_\theta}^{(2):SC} = \sum_{\theta' \neq \theta} \frac{\langle \Xi_{n_{\theta'}} | \Xi_{n_{\theta'}} \rangle}{E_{n_\theta}^{(0)} - E_{n_{\theta'}}^{SC}} = \sum_{\theta' \neq \theta} E_{\theta'}. \quad (24)$$

There are many possible ways to select important configurations using this second-order correction, but a straightforward approach is to select irreducible representations θ' with

$$\left| \frac{E_{\theta'}}{E_{n_\theta}^{(0)}} \right| > \epsilon_1, \quad (25)$$

where ϵ_1 is a small cutoff to regulate the number of irreps. We denote the number of irreps in SCI as N_θ , which is determined by ϵ_1 . For the state in the selected irreps,

$$|\Xi_{n_{\theta'}}\rangle = \sum_{I_{\theta'}} c_{I_{\theta'}} |\Phi_{I_{\theta'}}\rangle \quad (26)$$

we select the configurations with $|c_{I_{\theta'}}| > 0$.

We can further select the configurations by omitting those that contribute little to the state $|\Xi_{n_{\theta'}}\rangle$. That is, for the state in the selected irrep, $|\Xi_{n_{\theta'}}\rangle$ that satisfies Eq. (25), we choose the configurations with a coefficient larger than some cutoff ϵ_2 :

$$|c_{I_{\theta'}}| > \epsilon_2. \quad (27)$$

This condition is familiar from other calculations, including exact diagonalization using Davidson's method.

We can tweak these two parameters to select the number of configurations to fit within available computational resources. While one could vary ϵ_2 depending on the value of ϵ_1 , we consider ϵ_1 and ϵ_2 as fixed parameters. We make the selection criterion as simple as possible in this paper.

4.2 Quantum computing applications

Symmetry-based perturbation theory can be straightforwardly implemented in quantum computing applications. Once we obtain the second quantized Hamiltonian Eq. (6), we can transform it in terms of Pauli strings, $P_\alpha \in \{I, X, Y, Z\}^{\otimes N_Q}$:

$$H = \sum_{\alpha=1}^{N_P} c_\alpha P_\alpha. \quad (28)$$

The qubit Hamiltonian can then be simulated on quantum computers. The mapping to the qubit Hamiltonian is not unique and there are several methods. We consider the standard Jordan-Wigner transformation here, where the number of qubits N_Q equals the number of spin orbitals $2M$, and there is one-to-one correspondence between the occupation number states of a spin-orbital and the states of a qubit.

The \mathbb{Z}_2 symmetry operator in Eq. (21) can be written in the Jordan-Wigner transformation as

$$U_a = \prod_{p \in L_a} Z_p. \quad (29)$$

Z_p is a Pauli string where it is Z for the p -th qubit and I for the others. We consider K generators of the abelian group, U_a with $a = 1, \dots, K$. Since $[P_\alpha, U_a] = 0$ for all α and any U_a from Eq.(8), we can construct

a Clifford operator C using the K generators and perform the Clifford transformation on the Hamiltonian [69]:

$$H \rightarrow CHC^\dagger = \sum_{\alpha=1}^{N_P} c_\alpha Q_\alpha \quad (30)$$

where $Q_\alpha = CP_\alpha C^\dagger$ is a Pauli string with an overall + or - sign. Since the generator is in the Z operator basis as given in Eq. (29), we can show that there are K different $X_{q(i)}$ operators with $i = 1, 2, \dots, K$ for qubit index $q(i)$ such that $[Q_\alpha, X_{q(i)}] = 0$ for all α . This means that the eigenstate in Eq. (3) in the new basis, $C|\Psi_{n_\theta}\rangle$, is also an eigenstate of $X_{q(i)}$ for $i = 1, 2, \dots, K$, which can be uniquely determined by the irreducible representation θ of the state. Thus we can effectively reduce the number of qubits from N_Q to $N_Q - K$. This is called qubit tapering [69]. The relation of qubit tapering with the point group symmetry is further discussed in [70] and its application to chemistry problems is discussed in [71, 72].

If other transformations to the qubit Hamiltonian are related to the Jordan-Wigner transformation by a Clifford transformation, such as the Bravyi-Kitaev transformation, then the number of qubit tapering remains the same. For \mathbb{Z}_N symmetries with $N > 2$, the symmetry operator in the Jordan-Wigner transformation is in general written as a linear combination of multiple Pauli strings, and it cannot be used for qubit tapering in a way described above.

There are at least two \mathbb{Z}_2 symmetries associated with the spin and up to three additional \mathbb{Z}_2 symmetries associated with the exact point-group symmetry. The qubit tapering with the two \mathbb{Z}_2 symmetries of spin is associated with the Parity mapping, although it gives rise to two different Hamiltonians. The \mathbb{Z}_2 subgroups of the point group symmetry are the inversions and 180-degree rotations. Since there are three coordinates, $\mathbf{x} = (x, y, z)$, we can have at most three independent \mathbb{Z}_2 transformations, such as $\mathbf{x}_i \rightarrow -\mathbf{x}_i$ for each i . Therefore $K = 5$ is the maximum number possible in the electronic Hamiltonian.

Using SBPT, we can increase the number K of \mathbb{Z}_2 symmetries to any number up to N_Q . We consider additional generator U_b with $[H_{\text{ref}}, U_b] = 0$ but $[H, U_b] \neq 0$, where L_b is the set of spin orbitals that are nontrivially coupled as discussed in Sec. 3.1. Assuming that we have K' such additional generators, U_b with $b = 1, \dots, K'$, we can show that the optimal partitioning Eq. (10) can be translated into the Pauli string representation as

$$[P_\alpha, U_b] \neq 0 \quad (31)$$

for some U_b and for all P_α in H_{pert} . Again this optimal partitioning uniquely determines the reference Hamiltonian, as well as $V_{\theta', \theta}$ in Eq. (12). The reference Hamiltonian has K' additional generators, so we can reduce additional K' qubits.

SCI-SBPT2 in the previous section is also relevant in quantum computing applications. The use of selected CI in quantum computing applications was first proposed in [28] and was called quantum selected configuration interaction (QSCI). The SQD paper [33] extended QSCI and employed a recovery method, increasing the size of quantum circuits significantly on noisy quantum hardware. While SCI-SBPT2 can be implemented straightforwardly in QSCI, the recovery method in SQD needs modification since the number of particles is not well defined. The same issue arises for the Parity mapping. However, SCI-SBPT2 without qubit tapering can be used in both QSCI and SQD, and it can reduce the number of configurations in H_{ref} to select from samples obtained from quantum hardware run.

5 Results

In this section, we apply second-order symmetry-based perturbation theory (SBPT2) to the ground-state potential energy curves of two molecules, H_2O and N_2 , in the STO-3G basis. Through the examples, we show how SBPT2 works for systems with different point-group symmetries and demonstrate that SBPT2 can give accurate results with a lower computational cost than second-order n-electron valence state perturbation theory (NEVPT2). We measure the computational cost by the number of configurations and the number of qubits required to solve for H_{ref} . We also discuss N_2 in the 6-31G basis at the end.

We obtain the restricted Hartree-Fock orbitals with point-group symmetries using the free open-source chemistry software PySCF [73]. We have used PySCF to compute the exact energy dissociation curves, second-order Moller-Plesset perturbation theory (MP2), as well as the standard NEVPT2 calculations based

on the Dyall Hamiltonian with the strongly-contracted method. We denote NEVPT2 with CAS(N,M) as NEVPT2(N,M), where N is the number of electrons and M the number of orbitals.

For the other calculations, we have used the Jordan-Wigner transformation of the second-quantized Hamiltonian in terms of Pauli strings as in Sec. 4.2. As discussed above, we can use other transformations or the second quantized Hamiltonian directly, and the results will be independent of the basis. For the SBPT calculations, including a version of NEVPT2 based on the projection Hamiltonian, we have used the Epstein-Nesbet (EN) and strongly contracted (SC) approximations given in Eqs. (17) and (20), as well as the full uncontracted (UC) second-order correction (16). The UC correction is not scalable as discussed above, but the purpose of showing it for the small systems is to validate the SC approximation. The SCI-SBPT2 calculation is based on the SC approximation of the second-order correction.

5.1 H₂O

We start with the ground state energy dissociation curve for the water molecule in the STO-3G basis. We keep the angle between the two hydrogen atoms to be 104.5° and stretch the two O – H bonds. This ensures that the ground state has multi-reference character at large bond distances. To demonstrate the use of approximate point-group symmetries discussed in Sec. 3.1, we stretch one of the O – H bonds slightly more than the other: one bond length is set to be r while the other to be $r + \Delta r$ with a small deformation $\Delta r = 0.01$. We use the angstrom as the unit of length in this paper.

In the STO-3G basis with one frozen core, there are 6 orbitals and 8 electrons. The frozen-core approximation for the energy dissociation curve, which we treat as the exact solution, is given in Fig. 5a. We compute various perturbative approximations of the energy at 11 values of r equally spaced from $r = 0.6$ to $r = 2.6$. Figure 5a shows that the NEVPT2(4,3), MP2, and second-order Epstein-Nesbet perturbation theory (ENPT2) results have good agreement near the equilibrium geometry, but they deviate significantly from the exact solution both at large bond lengths as the system exhibits the multi-reference nature and at the dissociation limit. This plot shows that single-reference perturbation theory (SRPT) or multi-reference perturbation theory (MRPT) with small active space cannot correctly compute the dissociation curve.

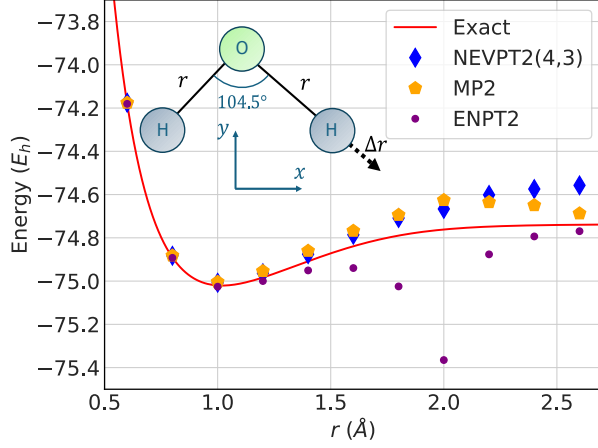
The point group symmetry of the H₂O molecule without the deformation, $\Delta r = 0$, is C_{2v} . There are two \mathbb{Z}_2 subgroups associated with the reflections σ_{xy} and σ_{yz} . One of them, σ_{yz} , is explicitly broken in the presence of the deformation $\Delta r \neq 0$. It is, however, an approximate symmetry when Δr is sufficiently small. We group the orbitals that transform nontrivially under the exact symmetry σ_{xy} in the solid box, and the approximate symmetry σ_{yz} , as well as the approximate \mathbb{Z}_2 symmetry for the lowest orbital that is weakly coupled, in the dotted boxes as shown in Fig. 5b. There are a multiple energy level crossings of the orbitals, and the orbital energy diagram is for $r = 1.8$. In the exact case, the number of configurations that respect the \mathbb{Z}_2 reflection symmetry associated with σ_{xy} and the two spin symmetries is 125. Since there are six orbitals, the number of qubits in the Jordan-Wigner transformation gives rise to 12 qubits. Using the three \mathbb{Z}_2 symmetries, we can reduce the number of qubits to 9. The summary of the resource requirements is given in Table 1.

	Exact	CAS(4,4)	SBPT	CAS(4,3)
Number of orbitals (M)	6	4	4	3
Number of qubits (N_Q)	9	6	4	4
Number of configs (N_{det})	125	36	16	9

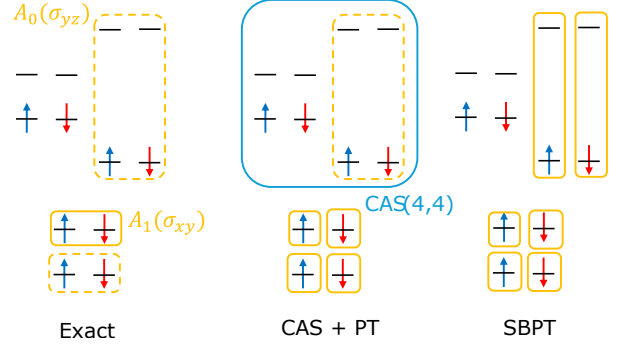
Table 1: The resource requirements - the number of qubits and configurations - for H₂O with the deformation in the STO-3G basis for the Hamiltonians defined in Fig. 5b. The exact case is the frozen core approximation, i.e. CAS(8,6). CAS(4,3) is for reference purposes. The table is ordered by increasing number of symmetries.

We now look for a good perturbative approximation of the dissociation curve with as few resources as possible. In other words, we aim to find a good reference Hamiltonian with the largest number of \mathbb{Z}_2 symmetries.

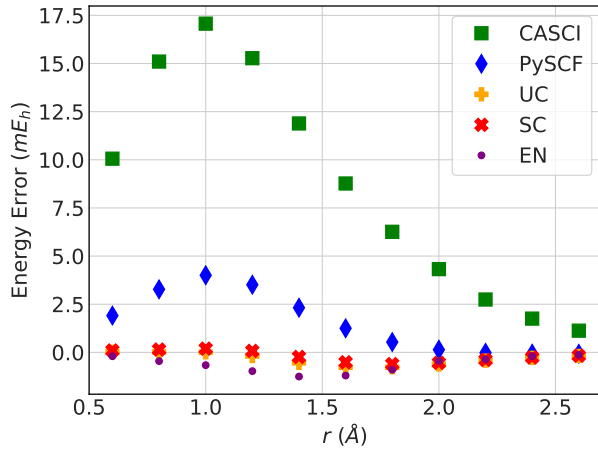
We can start with the conventional valence space to form the complete active space, CAS(4,4), and treat the two lowest orbitals as external orbitals as they are weakly coupled. This is the standard MRPT approach based on CASCI, and its orbital energy diagram with the \mathbb{Z}_2 symmetries is shown in the middle figure of



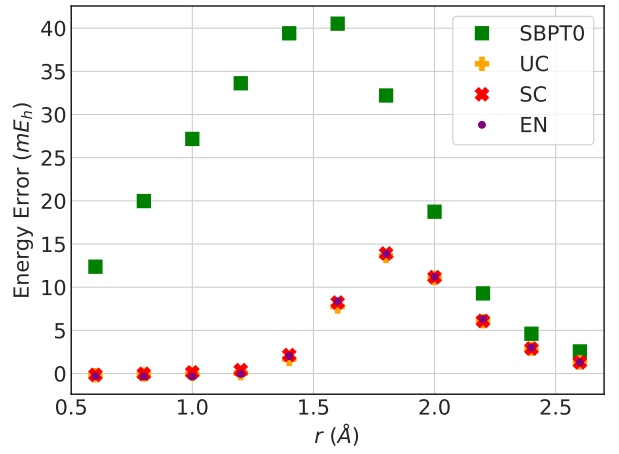
(a) Dissociation curve



(b) Orbital energy diagrams in MRPTs



(c) NEVPT2(4,4)



(d) SBPT2

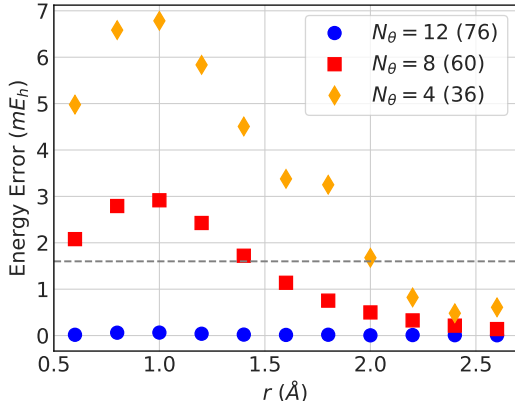
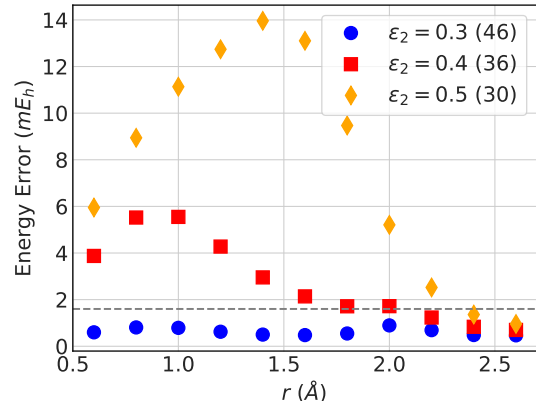
(e) SCI-SBPT2: $\epsilon_2 = 0$ (f) SCI-SBPT2: $N_\theta = 12$

Figure 5: Ground-state potential energy curve of H_2O in the STO-3G basis. (a) The dissociation curve for the deformed geometry, $\Delta r = 0.01$. (b) Schematic orbital energy diagrams for $r = 1.8$ with the groupings of the exact (solid) and approximate (dashed) \mathbb{Z}_2 symmetries in MRPTs. (c, d) NEVPT2(4,4) and SBPT2 results of the leading-order contributions and the 2nd order corrections: the uncontracted (UC), strongly-contracted (SC), and Epstein-Nesbet (EN) approximations are given in Eqs. (16), (20), and (17), respectively. PySCF uses the Dyall Hamiltonian with the SC approximation. (e, f) The SCI-SBPT2 results using the cutoffs given in Eqs. (25) and (27): varying ϵ_1 with fixed $\epsilon_2 = 0$ and varying ϵ_2 with fixed ϵ_1 , which gives the number of irreps, $N_\theta = 12$. The number in parenthesis is the number of selected configurations.

Fig. 5b. Figure 5c shows that the NEVPT2(4,4) results with the different approximations for the second-order correction give good agreement with the exact solution. We have explicitly checked that CAS(4,4) is the smallest active space to obtain reasonable agreement with the exact solution. This is expected, as we need to include all the 2p orbitals to keep the rotational symmetry in the dissociation limit. In CAS(4,4), the number of configurations that respect the \mathbb{Z}_2 symmetries is 36, and the number of qubits after the qubit tapering is 6.

As just seen above, the standard MRPT approaches miss the opportunity to exploit the approximate symmetry of σ_{yz} , while SBPT can readily incorporate it in the reference Hamiltonian as the following. The two orbitals ϕ_p in the dashed box in CAS(4,4) transform nontrivially under the reflection in the $y-z$ plane, $\phi_p \rightarrow -\phi_p + \Delta\phi_p$ where $|\Delta\phi_p| \ll |\phi_p|$. The deviation $\Delta\phi_p$ goes to zero as we take Δr to be zero. We consider the reference Hamiltonian that gives this approximate symmetry exact. This corresponds to the replacement of the dashed box with a solid box, resulting in the reduction of one extra qubit. Since the two orbitals in $A_0(\sigma_{yz})$ are weakly coupled to the rest of the orbitals, we can further decompose the exact symmetry as shown in the right figure of Fig. 5b. This corresponds to the reduction of two extra qubits in total, which is the same amount of reduction as CAS(4,3). Alternatively, we could divide A_0 as A_2 in Fig. 4, but this would give bad results at large bond lengths for two reasons. First the norm of the perturbation in the alternative grouping is larger, and second the grouping does not allow the spin singlet configurations, which are important in the dissociation limit. Therefore both the norm and chemistry arguments can correctly guide us to choose a better reference Hamiltonian in this example.

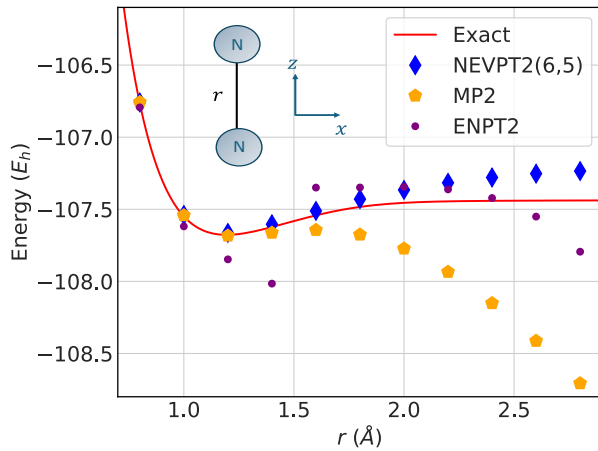
We find from Fig. 5d that the SBPT2 approximations agree well with the exact solution at all bond lengths. We also observe that the SC and EN approximations give the same results as the UC correction. This suggests that while the unperturbed state requires the reference Hamiltonian that incorporates multi-reference nature, each excited state in the reference Hamiltonian can be approximated in the mean-field approach with a single Slater determinant. In the intermediate range of the bond lengths where the correlation becomes strong, we see larger energy errors, but they are comparable to NEVPT2(4,4). In summary, SBPT2 and NEVPT2(4,4) both give good approximations, but SBPT2 can perform with a smaller computational cost than NEVPT2(4,4) by exploiting the approximate reflection symmetry.

As discussed in Sec. 4.1, all perturbative results are neither variational, as shown in Fig. 5, or convergent, even if we perform higher-order corrections. To achieve more accurate and systematic results, we could turn to SCI-SBPT2, where the results are shown in Figs. 5e and 5f with the dotted line indicating the kcal/mol accuracy, $1.6 mE_h$, as a reference point. We select configurations at $r = 1.8$ and use the same configurations for all the other values of r for simplicity. There are 125 configurations that respect the exact \mathbb{Z}_2 symmetries. The exact diagonalization of the ground state energy shows that we only need at most 30 out of 125 configurations to achieve the accuracy. With the augmented \mathbb{Z}_2 symmetry in SBPT, these 125 configurations belong to 25 different irreducible representations. With zero cutoffs $\epsilon_1 = \epsilon_2 = 0$, SCI-SBPT2 selects 116 configurations in 20 irreps. Figure 5e shows that at most 12 out of 20 irreps are relevant for the dissociation curve calculation. Moreover, we see from Fig. 5f that only 36 configurations in the 12 irreps can achieve the accuracy at $r = 1.8$, which is comparable to the required number of configurations from the exact diagonalization.

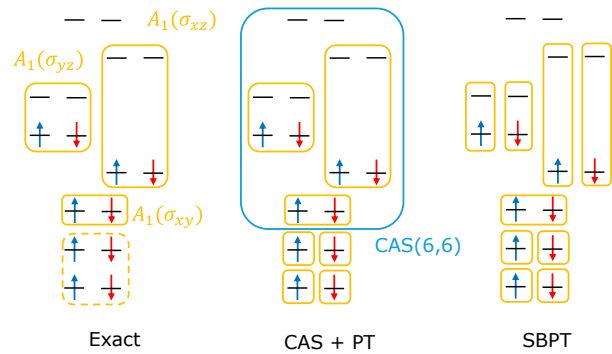
5.2 N_2

Next we compute the ground state energy dissociation curve for the nitrogen molecule in the STO-3G basis. It is well known that the dissociation of the molecule gives rise to multi-reference electronic wavefunctions, and therefore it is an ideal problem to compare different MRPTs. In the STO-3G basis with two core orbitals frozen, there are 8 molecular orbitals and 10 electrons. The dissociation curve of the ground state energy is plotted in Fig. 6a. We treat this as the exact solution, and we compare it with various perturbative approximations at 11 values of r equally spaced from $r = 0.8$ to $r = 2.8$. Figure 6a again shows that the SRPTs and MRPTs with a small active space breaks down at large bond lengths.

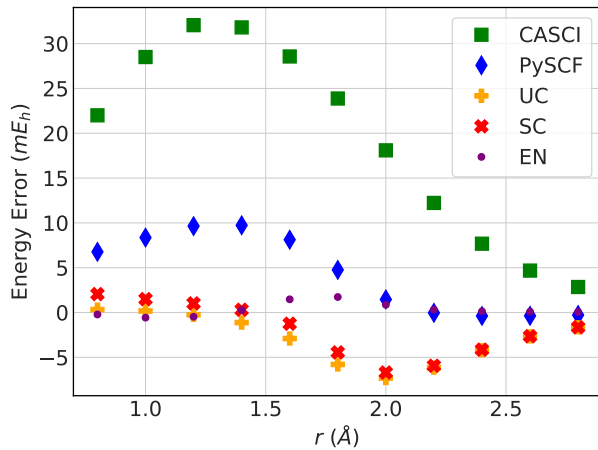
The point group symmetry of the N_2 molecule is $D_{\infty h}$. There are three \mathbb{Z}_2 subgroups associated with the reflection symmetries σ_{xy} , σ_{xz} , and σ_{yz} . We group the orbitals that transform nontrivially under these reflections as shown in Fig. 6b for $r = 1.8$ and label the grouping as $A_1(\sigma_{xy})$, etc. The lowest orbital in the core belongs to $A_1(\sigma_{xy})$, but we omit it in the figure to avoid cluttering. In the exact case, the number of configurations that respect these three \mathbb{Z}_2 symmetries, as well as the fixed number of spin up and down



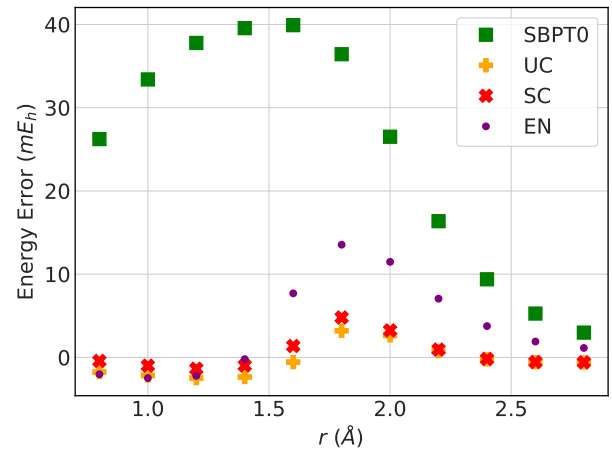
(a) Dissociation curve



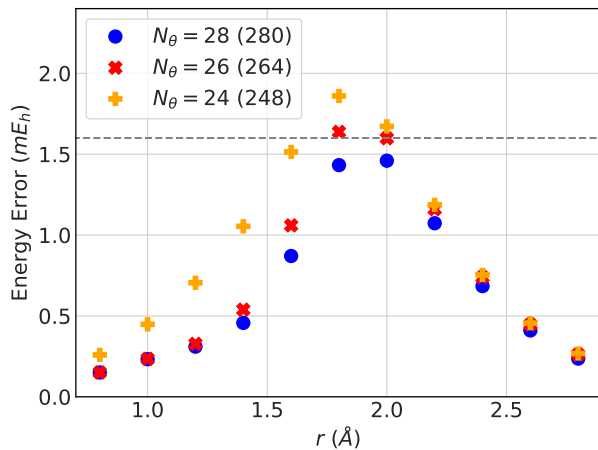
(b) Orbital energy diagrams in MRPTs



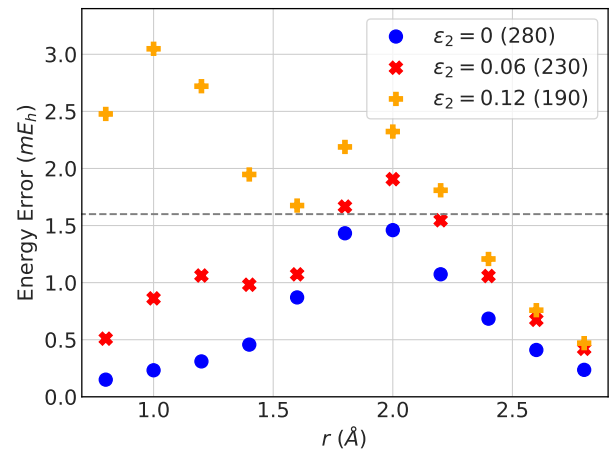
(c) NEVPT2(6,6)



(d) SBPT2



(e) SCI-SBPT2: $\epsilon_2 = 0$



(f) SCI-SBPT2: $\epsilon_1 = 0$

Figure 6: The ground state energy dissociation curve of N_2 in the STO-3G basis with various approximations similar to Fig. 5.

electrons, is 396. Since there are 8 orbitals, the Jordan-Wigner transformation gives rise to 16 qubits. Using the five \mathbb{Z}_2 symmetries, we can reduce the number of required qubits to 11 using the qubit tapering. The summary of the resource requirements is given in Table 2.

	Exact	CAS(6,6)	CAS(6,5)	SBPT
Number of orbitals (M)	8	6	5	6
Number of qubits (N_Q)	11	7	6	5
Number of configs (N_{det})	396	56	16	32

Table 2: The resource requirements - the number of qubits and configurations - for N_2 in the STO-3G basis for the Hamiltonians defined in Fig. 6b. The exact case is the frozen core approximation, i.e. CAS(10,8). The CAS(6,5) is included for reference purposes.

In the standard MRPT approaches, we can treat the two lowest orbitals as external orbitals as they are weakly coupled. Using the six 2p orbitals shown in the middle figure of Fig. 6b, we construct CAS(6,6) as the reference Hamiltonian. This gives a good agreement with the exact solution as shown in Fig. 6c, and in fact it is the smallest CAS for NEVPT2 that gives reasonable results. As we try to add additional external orbitals, they all give poor results, since we need all 2p orbitals to capture the correct physics.

We now apply SBPT2 to this problem. As in NEVPT2, we treat the two lowest orbitals as external orbitals. As discussed in Sec. 3.1, we need to find orbitals that are non-trivially coupled. Similar to the case of H_2O , we can take the groupings, $A_1(\sigma_{yz})$ and $A_1(\sigma_{xz})$, and split each grouping into half as shown in the right figure of Fig. 6b, using the same norm and chemistry arguments as before. As a result, there are two additional exact \mathbb{Z}_2 symmetries in the reference Hamiltonian, which is equivalent to reducing one additional orbital out of CAS(6,6) in terms of the qubit count. Using SBPT, we see that the second-order correction gives good agreement with the exact solution as shown in Fig. 6d. For both SBPT2 and NEVPT2, the mean-field treatment of the excited states, the EN approximation, gives larger errors and deviations from the full UC second-order correction compared to the SC approximation. This suggests that N_2 has a stronger multi-reference character than H_2O . The plot shows again that SBPT2 can perform as good as NEVPT2 but with smaller resource requirements for configurations and qubits.

Figures 6e and 6f show the results of SCI-SBPT for various cutoffs in Eqs. (25) and (27), where the dotted line indicates the kcal/mol accuracy, $1.6mE_h$. Again we select configurations based on one value of r and use the same configurations for the other values of r for simplicity. We have chosen $r = 1.8$ as the selection point because this is where the system exhibits multi-reference character. With zero cutoffs $\epsilon_1 = \epsilon_2 = 0$, there are 280 configurations in 28 irreps out of 396 configurations in 55 irreps. Both figures show a consistent improvement as we decrease the cutoffs, and the error is always positive, demonstrating that the method is both convergent and variational. From Fig. 6e, we see that all 28 irreps are important to achieve the accuracy, suggesting that CAS(6,6) is indeed the minimum active space to capture the correct physics. Within the 28 irreps, we can still select important configurations using the ϵ_2 cutoff, reducing the number of configurations from 280 to around 230 to achieve the accuracy for $r = 1.8$, as shown in Fig. 6f. The exact diagonalization of the ground state energy shows that we need at most 140 out of 396 configurations to achieve the accuracy for $r = 1.8$. This suggests that the selection of 28 irreps by SCI-SBPT2 misses some important configurations and requires us to select more configurations to achieve the same accuracy. This is another indication that the problem has a strong multi-reference character. Also the plots show that the selected configurations at one point may not work well at different points. We could overcome this problem by selecting important configurations from different values of r .

Lastly, we show some results of the ground state energy dissociation curve of N_2 in the 6-31G basis. In this case, there are 18 orbitals and 14 electrons. By freezing two core orbitals, we have 16 orbitals and 10 electrons. We treat the freezing core approximation as the exact solution and compare it with NEVPT2 and SBPT2 approximations. The resource requirements are shown in Table 3. From Fig. 7b, we find that although NEVPT2(6,6) gives a reasonable result with the same computational resources as before, it struggles in the dissociation limit. The larger active space size NEVPT2(6,14), which includes 3s and 3p orbitals, does not give a significant improvement. We have also found that NEVPT2(6,12) gives a similar result as NEVPT2(6,14). This suggests that all 16 orbitals need to be included in order to have a better

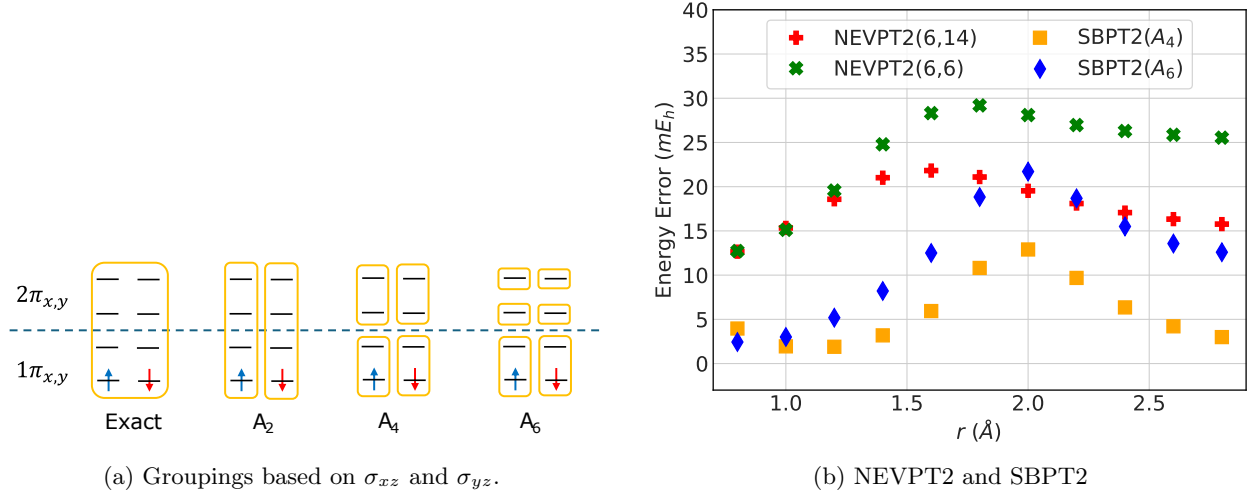


Figure 7: NEVPT2 and SBPT2 results for the ground state energy dissociation curve for N_2 in the 6-31G basis. We have used PySCF for NEVPT2 and the strongly-contracted approximation in Eq. (20) with two different groupings A_4 and A_6 for SBPT2.

result than NEVPT2.

	Exact	CAS(6,14)	SBPT(A_4)	SBPT(A_6)	CAS(6,6)
Number of orbitals (M)	16	14	16	16	6
Number of qubits (N_Q)	27	23	21	17	7
Number of configs (N_{det})	2,388,528	16,584	41,472	25,088	56

Table 3: The resource requirements - the number of qubits and configurations - for N_2 in the 6-31G basis. SBPT2 uses the groupings, A_4 and A_6 , shown in Fig. 7a. The exact case is the frozen core approximation, i.e. CAS(10,16).

We therefore perform SBPT2 on CAS(10,16). As mentioned above, there are three \mathbb{Z}_2 subgroups associated with the three reflection symmetries σ_{xy} , σ_{xz} , and σ_{yz} . The orbitals that transform nontrivially under these symmetries are doubled due to the $3s$ and $3p$ orbitals. For simplicity, we consider σ_{xz} and σ_{yz} symmetries, where the $\pi_{x,y}$ orbitals, which are linear combinations of $2p_{x,y}$ and $3p_{x,y}$, transform nontrivially, as shown in Fig. 7a. The study of the STO-3G basis would suggest that we could augment the symmetry using the grouping A_2 . In this case, we only have two extra symmetries as in the STO-3G basis, while the number of orbitals is doubled. This would not be favorable for scaling.

In this larger basis set, it is clear that we now have more ways to group the orbitals. The grouping A_4 in Fig. 7a is one of them. It is natural to group the $1\pi_{x,y}$ orbitals as in A_4 using the argument from the STO-3G case. As for $2\pi_{x,y}$, we have chosen this grouping because it gives the smaller norm of the perturbation than other groupings, such as A_2 in Fig. 4. The result is plotted as the orange square in Fig. 7b, which shows a better result than the NEVPT2 results. In this case, we have 6 additional symmetries, compared to 2 in the STO-3G basis. Even though the number of orbitals in CAS(10,16) is nearly triple that of CAS(6,6) in the STO-3G basis, the number of additional symmetries is also triple. As we further increase the number of symmetries as in A_6 , the result gets worse, showing that the contribution of $2\pi_{x,y}$ orbitals is important for better accuracy. This example demonstrates that the number of symmetries can increase in SBPT2 as we expand the basis set.

6 Conclusions

We have developed a multi-reference perturbation theory based on symmetries of the electronic Hamiltonian. This symmetry-based perturbation theory (SBPT) extends existing perturbation theories to include other forms of the reference Hamiltonian.

We have argued that we can use SBPT when some spin orbitals are weakly coupled due to approximate symmetries. There is an optimal way to construct the reference Hamiltonian based on the symmetries, and in this construction we can use the strongly-contracted method, which gives a scalable approximation to higher-order corrections.

We have formulated SBPT in the context of qubit operators for quantum computing applications. The augmented \mathbb{Z}_2 symmetry can reduce the qubit count via qubit tapering. We have also applied SBPT2 to SCI in order to overcome the shortcomings of perturbation theories and obtained the convergent and variational results.

We have applied our methods to N_2 and H_2O in the STO-3G basis. By solving these small systems, we have explained our approach in detail and shown that SBPT2 can give accurate results with fewer configurations and qubits than NEVPT2. We have further studied N_2 in the 6-31G basis and found that we can add more symmetries in the reference Hamiltonian in the larger basis set, providing an evidence that SBPT2 can be effective for larger systems. The systematic exploration of how SBPT2 results depend on the construction of the reference Hamiltonian in larger molecular systems needs further investigation.

Acknowledgements

We would like to thank Jay Lowell and Marna Kagele in the DC&N organization at Boeing for supporting this work. We acknowledge Julia Rice, Ben Link, and Triet Friedhoff for numerous helpful discussions and James Shee for valuable feedback on the manuscript.

References

- [1] Kristen S. Williams, Joseph P. Labukas, Victor Rodriguez-Santiago, and Jan W. Andzelm. First principles modeling of water dissociation on mg(0001) and development of a mg surface pourbaix diagram. *Corrosion*, 71(2):209–223, 2015.
- [2] Eno E. Ebenso, Chandrabhan Verma, Lukman O. Olasunkanmi, Ekemini D. Akpan, Dakeshwar Kumar Verma, Hassane Lgaz, Lei Guo, Savas Kaya, and M. A. Quraishi. Molecular modelling of compounds used for corrosion inhibition studies: a review. *Phys. Chem. Chem. Phys.*, 23:19987–20027, 2021.
- [3] Na Sai, Kevin Leung, Judit Zádor, and Graeme Henkelman. First principles study of photo-oxidation degradation mechanisms in p3ht for organic solar cells. *Phys. Chem. Chem. Phys.*, 16:8092–8099, 2014.
- [4] Yidong Zhou, Jintai Chen, Jinglei Cheng, Xu Cao, Yuanyuan Zhang, Gopal Karemore, Marinka Zitnik, Frederic T. Chong, Junyu Liu, Tianfan Fu, and Zhiding Liang. Quantum-machine-assisted drug discovery. *npj Drug Discovery*, 3, 2026.
- [5] Anastasiia V. Sadybekov and Vsevolod Katritch. Computational approaches streamlining drug discovery. *Nature*, 616:673–685, 2023.
- [6] Mahesh Datt Bhatt and Colm O’Dwyer. Recent progress in theoretical and computational investigations of li-ion battery materials and electrolytes. *Phys. Chem. Chem. Phys.*, 17:4799–4844, 2015.
- [7] H. Bethe. Zur theorie der metalle. *Zeitschrift für Physik*, 71:205–226, 1931.
- [8] Chr. Knakkegård Møller and Milton S. Plesset. Note on an approximation treatment for many-electron systems. *Physical Review*, 46:618–622, 1934.
- [9] Paul S. Epstein. The stark effect from the point of view of schroedinger’s quantum theory. *Physical Review*, 28:695–710, 1926.

- [10] Robert K. Nesbet. Configuration interaction in orbital theories. *Proceedings of the Royal Society of London. Series A. Mathematical and Physical Sciences*, 230:312 – 321, 1955.
- [11] Ireneusz W. Bulik, Thomas M. Henderson, and Gustavo E. Scuseria. Can single-reference coupled cluster theory describe static correlation? *J. Chem. Theory Comput.*, 11:3171–3179, 2015.
- [12] Sandeep Sharma, Kantharuban Sivalingam, Frank Neese, and Garnet Kin-Lic Chan. Low-energy spectrum of iron–sulfur clusters directly from many-particle quantum mechanics. *Nature Chemistry*, 6:927–933, 2014.
- [13] Yuki Kurashige, Garnet Kin-Lic Chan, and Takeshi Yanai. Entangled quantum electronic wavefunctions of the mn4cao5 cluster in photosystem ii. *Nature Chemistry*, 5:660–666, 2013.
- [14] Electronic landscape of the p-cluster of nitrogenase as revealed through many-electron quantum wavefunction simulations. *Nature Chemistry*, 11:1026–1033, 2019.
- [15] M. R. Norman. Colloquium: Herbertsmithite and the search for the quantum spin liquid. *Rev. Mod. Phys.*, 88:041002, Dec 2016.
- [16] Aron J. Cohen, Paula Mori-Sánchez, and Weitao Yang. Insights into current limitations of density functional theory. *Science*, 321(5890):792–794, 2008.
- [17] Vladimir I. Anisimov, F. Aryasetiawan, and A. I. Lichtenstein. First-principles calculations of the electronic structure and spectra of strongly correlated systems: the lda+u method. *Journal of Physics: Condensed Matter*, 9(4):767, 1997.
- [18] Björn Roos, Per Linse, Per E. M. Siegbahn, and Margareta R. A. Blomberg. A simple method for the evaluation of the second-order-perturbation energy from external double-excitations with a casscf reference wavefunction. *Chemical Physics*, 66:197–207, 1982.
- [19] Celestino Angeli, Renzo Cimiraglia, Stefano Evangelisti, Thierry Leininger, and Jean-Paul Malrieu. Introduction of n-electron valence states for multireference perturbation theory. *Journal of Chemical Physics*, 114:10252–10264, 2001.
- [20] Celestino Angeli, Renzo Cimiraglia, and Jean-Paul Malrieu. N-electron valence state perturbation theory: a fast implementation of the strongly contracted variant. *Chemical Physics Letters*, 350:297–305, 2001.
- [21] Celestino Angeli, Renzo Cimiraglia, and Jean-Paul Malrieu. n-electron valence state perturbation theory: A spinless formulation and an efficient implementation of the strongly contracted and of the partially contracted variants. *Journal of Chemical Physics*, 117:9138–9153, 2002.
- [22] Alexei Y. Kitaev. Quantum measurements and the abelian stabilizer problem. *Electron. Colloquium Comput. Complex.*, TR96, 1995.
- [23] Alán Aspuru-Guzik, Anthony D. Dutoi, Peter J. Love, and Martin Head-Gordon. Simulated quantum computation of molecular energies. *Science*, 309:1704 – 1707, 2005.
- [24] Alberto Peruzzo, Jarrod McClean, Peter Shadbolt, Man-Hong Yung, Xiao-Qi Zhou, Peter J. Love, Alán Aspuru-Guzik, and Jeremy L. O’Brien. A variational eigenvalue solver on a photonic quantum processor. *Nature Communications*, 5, 2014.
- [25] Mario Motta, Kevin J Sung, K Birgitta Whaley, Martin Head-Gordon, and James Shee. Bridging physical intuition and hardware efficiency for correlated electronic states: the local unitary cluster Jastrow ansatz for electronic structure. *Chem. Sci*, 14(40):11213–11227, 2023.
- [26] Jeffery Yu, Javier Robledo Moreno, Joseph T. Iosue, Luke Bertels, Daniel Claudino, Bryce Fuller, Peter Groszkowski, Travis S. Humble, Petar Jurcevic, William Kirby, Thomas A. Maier, Mario Motta, Bibek Pokharel, Alireza Seif, Amir Shehata, Kevin J. Sung, Minh C. Tran, Vinay Tripathi, Antonio Mezzacapo, and Kunal Sharma. Quantum-centric algorithm for sample-based krylov diagonalization. *arXiv2501.09702*, 2025.

- [27] Nobuyuki Yoshioka, Mirko Amico, William Kirby, Petar Jurcevic, Arkopal Dutt, Bryce Fuller, Shelly Garion, Holger Haas, Ikko Hamamura, Alexander Ivrii, Ritajit Majumdar, Zlatko Minev, Mario Motta, Bibek Pokharel, Pedro Rivero, Kunal Sharma, Christopher J. Wood, Ali Javadi-Abhari, and Antonio Mezzacapo. Krylov diagonalization of large many-body hamiltonians on a quantum processor. *Nature Communications*, 16, 2025.
- [28] Keita Kanno, Masaya Kohda, Ryosuke Imai, Sho Koh, Kosuke Mitarai, Wataru Mizukami, and Yuya O Nakagawa. Quantum-selected configuration interaction: Classical diagonalization of hamiltonians in subspaces selected by quantum computers. *arXiv preprint arXiv:2302.11320*, 2023.
- [29] Yuya O. Nakagawa, Masahiko Kamoshita, Wataru Mizukami, Shotaro Sudo, and Yu ya Ohnishi. Adapt-qsci: Adaptive construction of an input state for quantum-selected configuration interaction. *Journal of chemical theory and computation*, 2023.
- [30] Kenji Sugisaki, Shu Kanno, Toshinari Itoko, Rei Sakuma, and Naoki Yamamoto. Hamiltonian simulation-based quantum-selected configuration interaction for large-scale electronic structure calculations with a quantum computer. *Phys. Chem. Chem. Phys.*, 27:20869–20884, 2025.
- [31] Mathias Mikkelsen and Yuya O Nakagawa. Quantum-selected configuration interaction with time-evolved state. *arXiv preprint arXiv:2412.13839*, 2024.
- [32] Soichi Shirai, Shih-Yen Tseng, Hokuto Iwakiri, Takahiro Horiba, Hiroto Hirai, and Sho Koh. Enhancing accuracy of quantum-selected configuration interaction calculations using multireference perturbation theory: Application to aromatic molecules. *ACS omega*, 10(35):39736–39750, 2025.
- [33] Javier Robledo-Moreno, Mario Motta, Holger Haas, Ali Javadi-Abhari, Petar Jurcevic, William Kirby, Simon Martiel, Kunal Sharma, Sandeep Sharma, Tomonori Shirakawa, Iskandar Sitdikov, Rong-Yang Sun, Kevin J. Sung, Maika Takita, Minh C. Tran, Seiji Yunoki, and Antonio Mezzacapo. Chemistry beyond the scale of exact diagonalization on a quantum-centric supercomputer. *Science Advances*, 11(25):eadu9991, 2025.
- [34] Danil Kaliakin, Akhil Shajan, Javier Robledo Moreno, Zhen Li, Abhishek Mitra, Mario Motta, Caleb Johnson, Abdullah Ash Saki, Susanta Das, Iskandar Sitdikov, Antonio Mezzacapo, and Kenneth M. Merz Jr. Accurate quantum-centric simulations of supramolecular interactions. *Communications Physics*, 8, 2025.
- [35] Ieva Liepuoniute, Kirstin D Doney, Javier Robledo-Moreno, Joshua A Job, Will S Friend, and Gavin O Jones. Quantum-centric computational study of methylene singlet and triplet states. *J. Chem. Theory Comput.*, 21:5062–5070, 2025.
- [36] Tyler Smith, Tanvi P. Gujarati, Mario Motta, Ben Link, Ieva Liepuoniute, Triet Friedhoff, Hiromichi Nishimura, Nam Nguyen, Kristen S. Williams, Javier Robledo Moreno, Caleb Johnson, Kevin J. Sung, Abdullah Ash Saki, and Marna Kagele. Quantum-centric simulation of hydrogen abstraction by sample-based quantum diagonalization and entanglement forging. *arXiv2508.08229*, 2025.
- [37] Marco Antonio Barroca, Tanvi Gujarati, Vidushi Sharma, Rodrigo Neumann Barros Ferreira, Young-Hye Na, Maxwell Giammona, Antonio Mezzacapo, Benjamin Wunsch, and Mathias Steiner. Scaling active spaces in simulations of surface reactions through sample-based quantum diagonalization. *arXiv2503.10923*, 2025.
- [38] Stefano Barison, Javier Robledo Moreno, and Mario Motta. Quantum-centric computation of molecular excited states with extended sample-based quantum diagonalization. 10(2):025034, 2025.
- [39] Saurabh Shivpuje, Tanvi P. Gujarati, Richard Van, Frank C. Pickard IV, Triet Friedhoff, Ieva Liepuoniute, Wade Davis, Gavin O. Jones, and Alexey Galda. Sample-based quantum diagonalization methods for modeling the photochemistry of diazirine and diazo compounds. *arXiv2510.00484*, 2025.

- [40] Alessandro Tammaro, Davide Emilio Galli, Julia E. Rice, and Mario Motta. N-electron valence perturbation theory with reference wave functions from quantum computing: Application to the relative stability of hydroxide anion and hydroxyl radical. *The journal of physical chemistry. A*, 2022.
- [41] Michal Krompiec and David Muñoz Ramo. Strongly contracted n-electron valence state perturbation theory using reduced density matrices from a quantum computer. 2022.
- [42] Attila Szabó and Neil S. Ostlund. Modern quantum chemistry : introduction to advanced electronic structure theory. 1982.
- [43] Trygve Helgaker, Poul Jørgensen, and Jeppe Olsen. Molecular electronic-structure theory. 2000.
- [44] F. Albert Cotton. Chemical applications of group theory. 1971.
- [45] Michael Tinkham. Group theory and quantum mechanics. 1964.
- [46] Smik Patel, Praveen Jayakumar, Rick Huang, Tao Zeng, and Artur F. Izmaylov. Quantum seniority-based subspace expansion: Linear combinations of short-circuit unitary transformations for the electronic structure problem. 2025.
- [47] Yinxuan Song, Yifan Cheng, Yingjin Ma, and Hai bo Ma. Multi-reference epstein–nesbet perturbation theory with density matrix renormalization group reference wavefunction. *Electronic Structure*, 2, 2019.
- [48] Kerstin Andersson, Per-Åke Malmqvist, and Björn O Roos. Second-order perturbation theory with a complete active space self-consistent field reference function. *The Journal of chemical physics*, 96(2):1218–1226, 1992.
- [49] Björn O Roos and Kerstin Andersson. Multiconfigurational perturbation theory with level shift—the cr2 potential revisited. *Chemical physics letters*, 245(2-3):215–223, 1995.
- [50] Niclas Forsberg and Per-Åke Malmqvist. Multiconfiguration perturbation theory with imaginary level shift. *Chemical Physics Letters*, 274(1-3):196–204, 1997.
- [51] Stefano Battaglia, Lina Fransén, Ignacio Fdez. Galván, and Roland Lindh. Regularized caspt2: An intruder-state-free approach. *Journal of Chemical Theory and Computation*, 18(8):4814–4825, 2022.
- [52] Celestino Angeli, Renzo Cimiraglia, and Jean-Paul Malrieu. N-electron valence state perturbation theory: a fast implementation of the strongly contracted variant. *Chemical physics letters*, 350(3-4):297–305, 2001.
- [53] Alexander Yu Sokolov. Multireference perturbation theories based on the dyall hamiltonian. *Advances in Quantum Chemistry*, 90:121–155, 2024.
- [54] Norm M Tubman, Joonho Lee, Tyler Y Takeshita, Martin Head-Gordon, and K Birgitta Whaley. A deterministic alternative to the full configuration interaction quantum monte carlo method. *The Journal of chemical physics*, 145(4), 2016.
- [55] Adam A Holmes, Norm M Tubman, and CJ Umrigar. Heat-bath configuration interaction: An efficient selected configuration interaction algorithm inspired by heat-bath sampling. *Journal of chemical theory and computation*, 12(8):3674–3680, 2016.
- [56] Jeffrey B Schriber and Francesco A Evangelista. Communication: An adaptive configuration interaction approach for strongly correlated electrons with tunable accuracy. *The Journal of chemical physics*, 144(16), 2016.
- [57] Hao Zhang and Matthew Otten. From random determinants to the ground state. *arXiv preprint arXiv:2511.14734*, 2025.
- [58] Charles F Bender and Ernest R Davidson. Studies in configuration interaction: The first-row diatomic hydrides. *Physical Review*, 183(1):23, 1969.

- [59] Bernard Huron, JP Malrieu, and P Rancurel. Iterative perturbation calculations of ground and excited state energies from multiconfigurational zeroth-order wavefunctions. *The Journal of Chemical Physics*, 58(12):5745–5759, 1973.
- [60] Robert J Buenker and Sigrid D Peyerimhoff. Individualized configuration selection in ci calculations with subsequent energy extrapolation. *Theoretica chimica acta*, 35(1):33–58, 1974.
- [61] Robert J Buenker, Sigrid D Peyerimhoff, and Werner Butscher. Applicability of the multi-reference double-excitation ci (mrd-ci) method to the calculation of electronic wavefunctions and comparison with related techniques. *Molecular Physics*, 35(3):771–791, 1978.
- [62] Stefano Evangelisti, Jean-Pierre Daudey, and Jean-Paul Malrieu. Convergence of an improved cipsi algorithm. *Chemical Physics*, 75(1):91–102, 1983.
- [63] F Illas, J Rubio, JM Ricart, and PS Bagus. Selected versus complete configuration interaction expansions. *The Journal of chemical physics*, 95(3):1877–1883, 1991.
- [64] Robert J Harrison. Approximating full configuration interaction with selected configuration interaction and perturbation theory. *The Journal of chemical physics*, 94(7):5021–5031, 1991.
- [65] Joseph Ivanic and Klaus Ruedenberg. Identification of deadwood in configuration spaces through general direct configuration interaction. *Theoretical Chemistry Accounts*, 106(5):339–351, 2001.
- [66] P Stampfuß and W Wenzel. Improved implementation and application of the individually selecting configuration interaction method. *The Journal of chemical physics*, 122(2):024110, 2005.
- [67] Laimutis Bytautas and Klaus Ruedenberg. A priori identification of configurational deadwood. *Chemical Physics*, 356(1-3):64–75, 2009.
- [68] Robert Roth. Importance truncation for large-scale configuration interaction approaches. *Physical Review C—Nuclear Physics*, 79(6):064324, 2009.
- [69] Sergey Bravyi, Jay M. Gambetta, Antonio Mezzacapo, and Kristan Temme. Tapering off qubits to simulate fermionic hamiltonians. *arXiv: Quantum Physics*, 2017.
- [70] Kanav Setia, Richard Chen, Julia E. Rice, Antonio Mezzacapo, Marco Pistoia, and James Daniel Whitfield. Reducing qubit requirements for quantum simulation using molecular point group symmetries. *Journal of chemical theory and computation*, 2019.
- [71] Ryan V. Mishmash, Tanvi P. Gujarati, Mario Motta, Huanchen Zhai, Garnet Kin-Lic Chan, and Antonio Mezzacapo. Hierarchical clifford transformations to reduce entanglement in quantum chemistry wave functions. *Journal of chemical theory and computation*, 2023.
- [72] Dario Picozzi and Jonathan Tennyson. Symmetry-adapted encodings for qubit number reduction by point-group and other boolean symmetries. *Quantum Science and Technology*, 8, 2023.
- [73] Qiming Sun, Timothy C. Berkelbach, Nick S. Blunt, George H. Booth, Sheng Guo, Zhendong Li, Junzi Liu, James D. McClain, Elvira R. Sayfutyarova, Sandeep Sharma, Sebastian Wouters, and Garnet Kin-Lic Chan. Pyscf: the python-based simulations of chemistry framework. *Wiley Interdisciplinary Reviews: Computational Molecular Science*, 8, 2017.